Supplement of Atmos. Chem. Phys., 25, 10707–10730, 2025
https://doi.org/10.5194/acp-25-10707-2025-supplement

Atmospheric Chemistry and Physics
Open Access
EGU

Supplement of

Evaluating NO_x fate and organic nitrate chemistry from α-pinene oxidation using stable oxygen and nitrogen isotopes

Wendell W. Walters et al.

Correspondence to: Wendell W. Walters (wendellw@mailbox.sc.edu)

Contents:

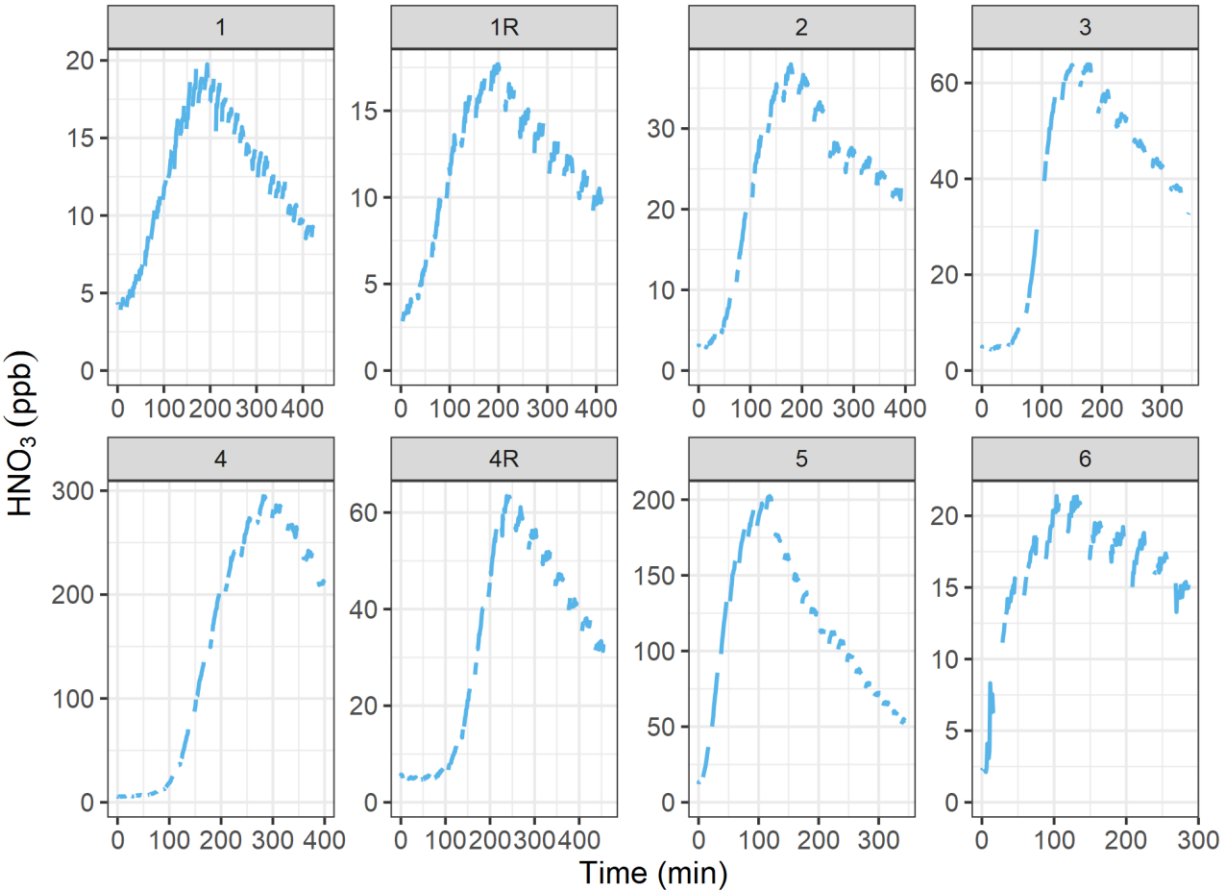

Fig. S1. The measured HNO_3 concentrations for the various conducted experiments. The measurements were made using CIMS. A substantial "chamber blank" was observed before the start (time = 0) of the experiments.

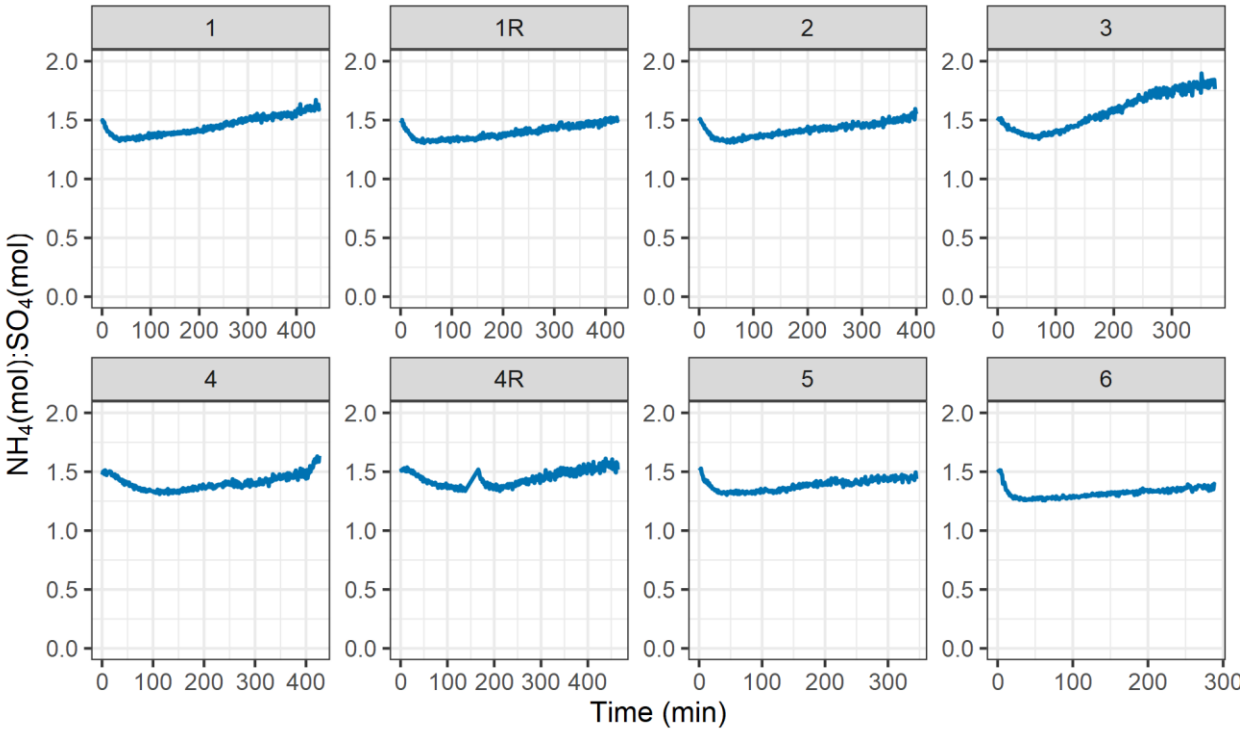

Fig. S2. The measured NH_4(mol):SO_4(mol) ratio for each conducted experiment from the HR-ToF-AMS. The ratios remained consistent and below 2 during the experiment indicative of minor contributions of pNO_3 derived from HNO_3.

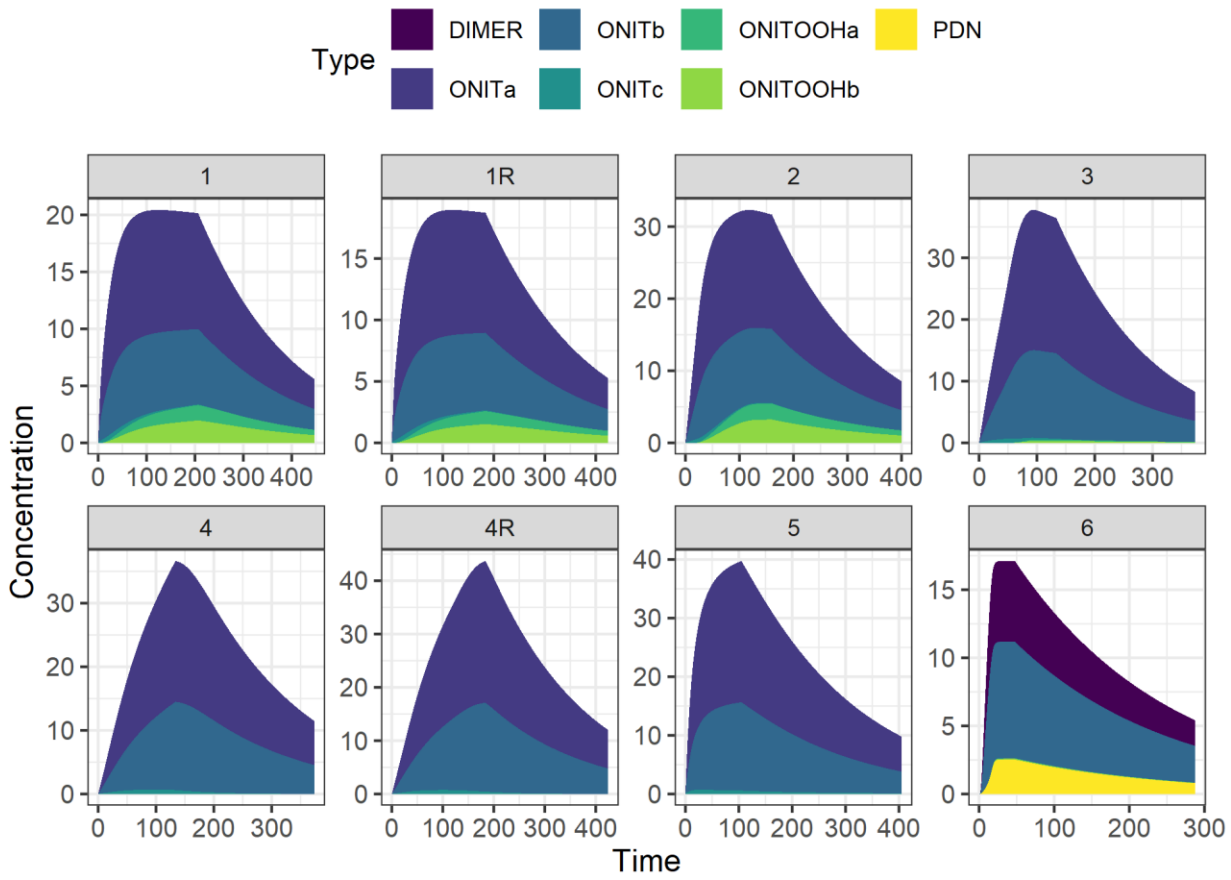

Fig. S3. The simulated types of organic nitrate and isomers formed during the various *α*-pinene/NO_x oxidation experiments using the NO_x-API mechanism. The mechanism includes 2 pinene hydroxyl-nitrate (ONITa (tertiary) and ONITb (secondary)), pinene carbonyl nitrate (ONITc), pinene nitrooxy-hydroperoxide (ONITOOHa (tertiary) and ONITOOHb (secondary)), dimer (DIMER), and pinene dinitrate (PDN).

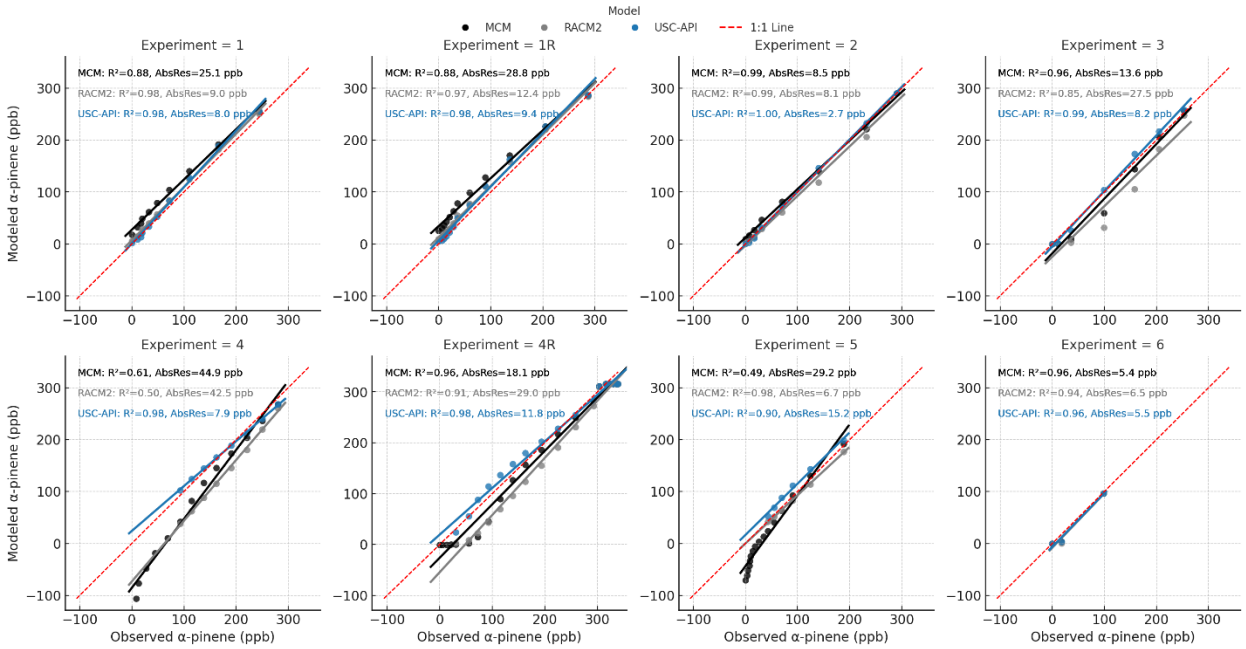

Fig. S4. Observed versus modeled concentrations of α-pinene across the chamber experiments. Model predictions are shown for three chemical mechanisms: MCM (black), RACM2 (grey), and NO_x-API(blue). The red line indicates the 1:1 reference. The coefficient of determination (R^2) and average absolute residual (AbsRes) are reported for each model. The R^2 values were calculated using the sklearn metric, which evaluates how well model predictions reproduce the observed values assuming a 1:1 relationship.

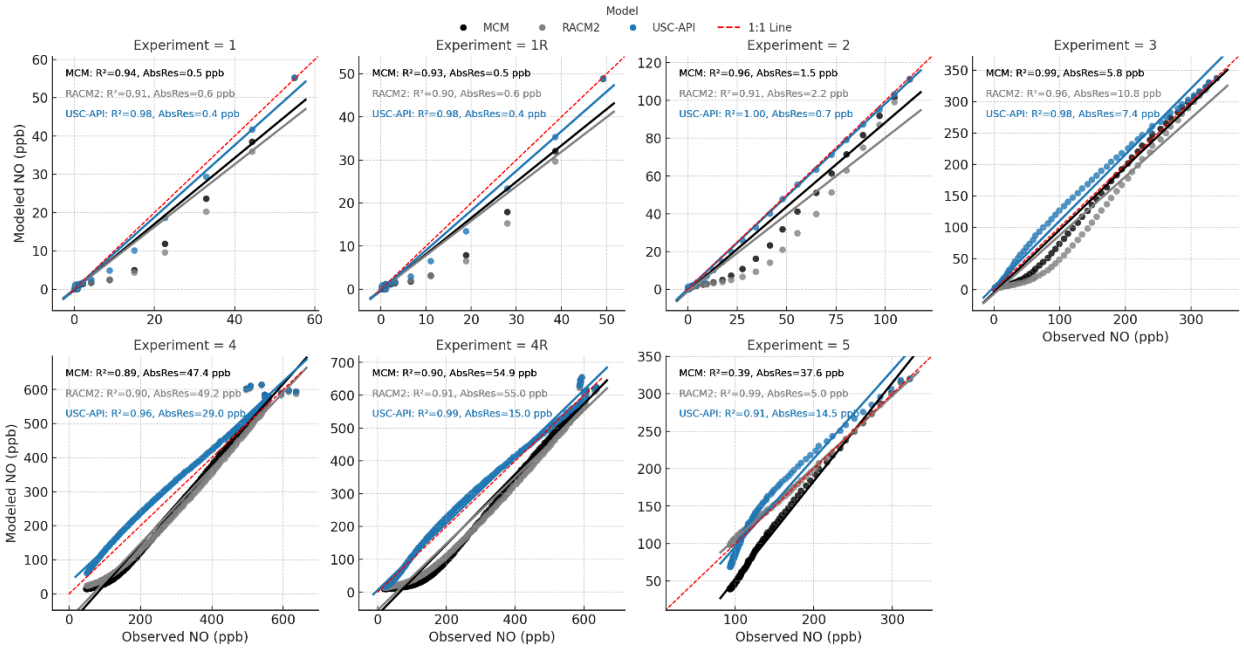

Fig. S5. Observed versus modeled concentrations of NO across the photochemical chamber experiments. Model predictions are shown for three chemical mechanisms: MCM (black), RACM2 (grey), and NO_x-API(blue). The red line indicates the 1:1 reference. The coefficient of determination (R^2) and average absolute residual (AbsRes) are reported for each model. The R^2 values were calculated using the sklearn metric, which evaluates how well model predictions reproduce the observed values assuming a 1:1 relationship. Experiment 6 (nighttime oxidation) was omitted from the analysis as NO was not among the initial reactants.

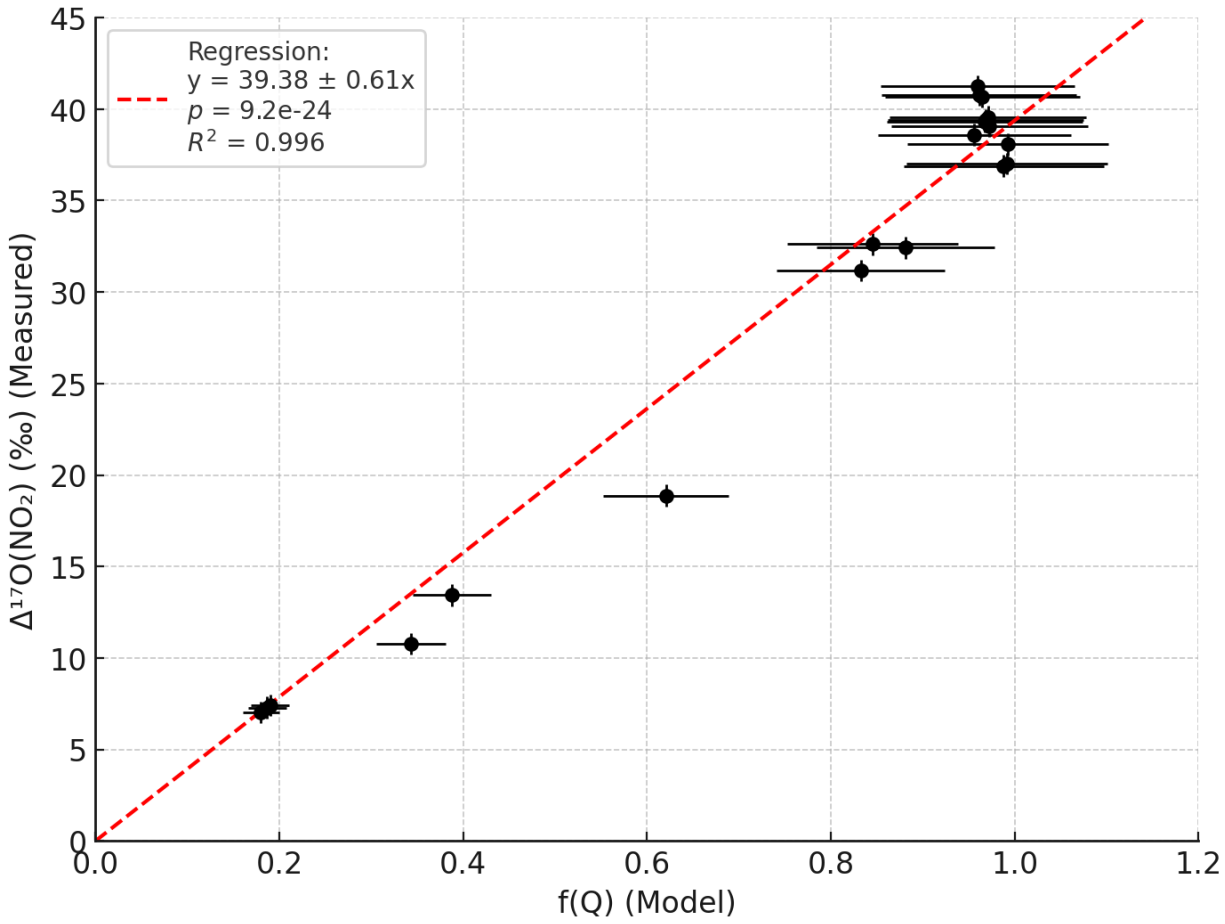

Fig. S6. Relationship between measured $\Delta^{17}O(NO_2)$ and the modeled fraction of NO_2 produced via ozone oxidation (f(Q)) across all experiments. Black circles represent measured $\Delta^{17}O(NO_2)$ values with ±0.7 ‰ uncertainty. The red dashed line shows the linear regression.

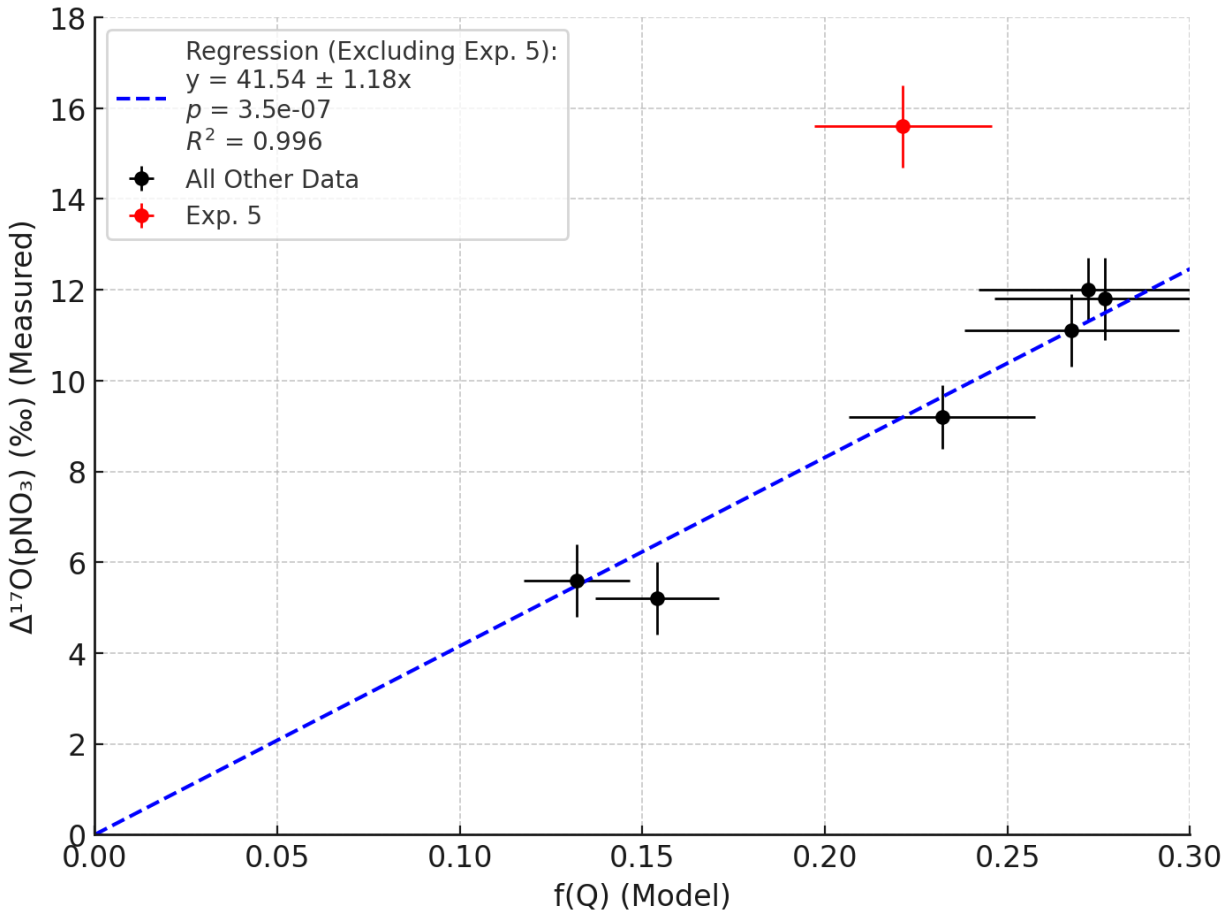

Fig. S7. The measured $\Delta^{17}O(pNO_3)$ versus modeled $f(Q)$ for all experiments. Black circles represent measurements with 1σ uncertainty, while the red circle highlights Exp. 5. The linear regressions (blue dashed line) excludes Exp. 5.

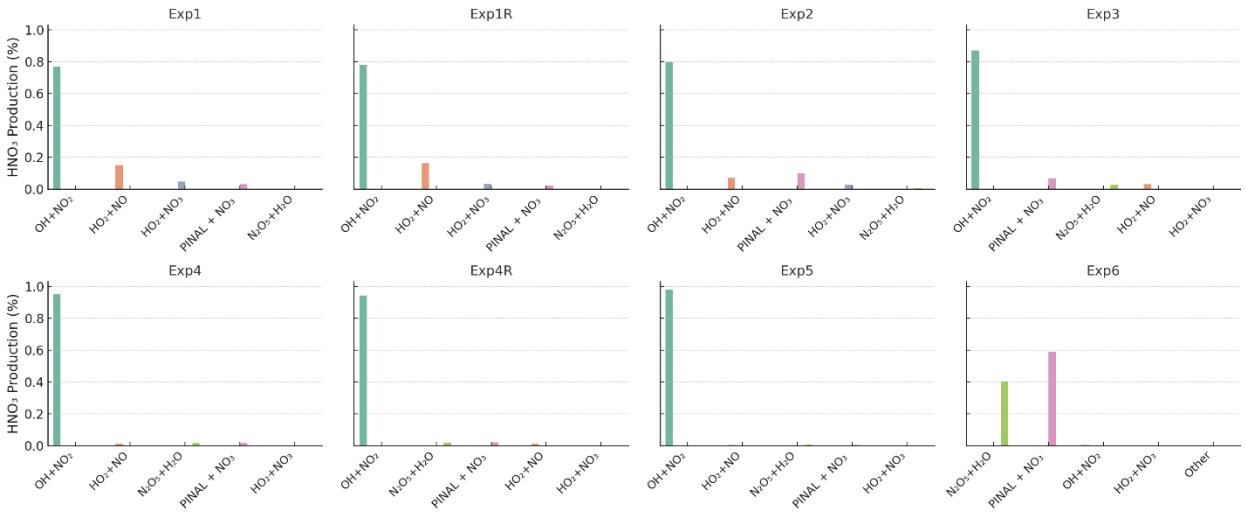

Fig. S8. Modeled contributions of individual chemical pathways to HNO_3 production for each chamber experiment using the NO_x-API base mechanism.

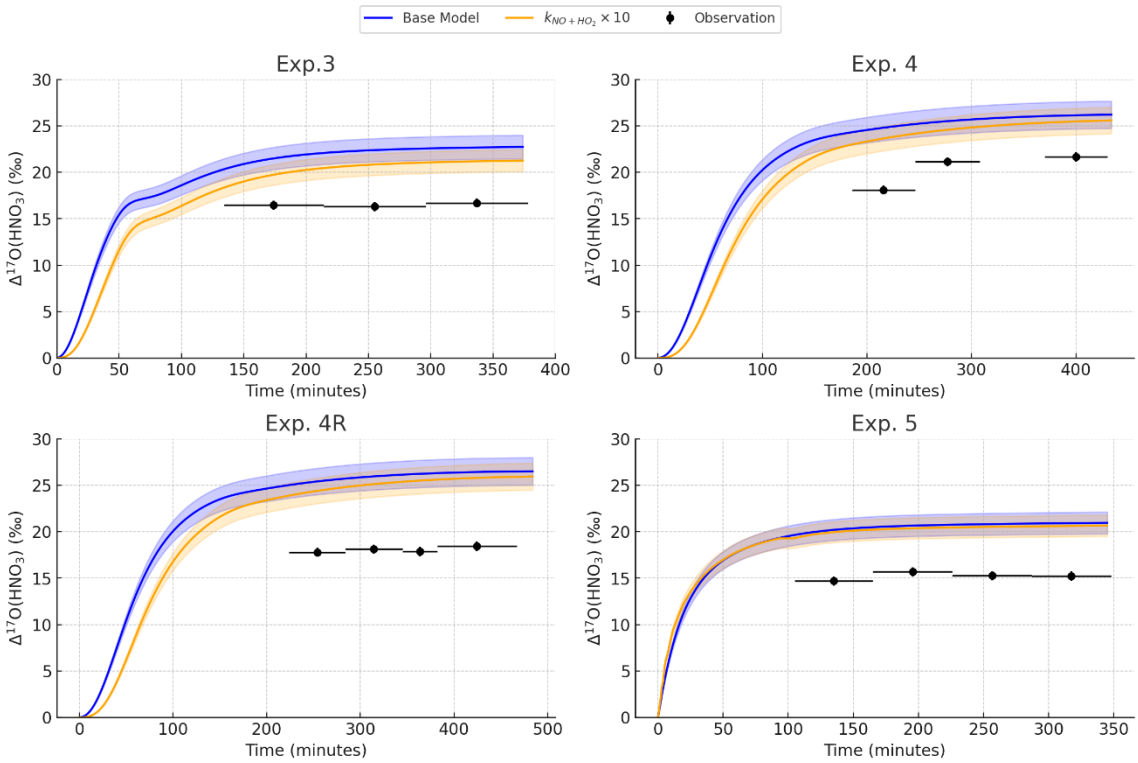

Fig. S9. Modeled and observed $\Delta^{17}O(HNO_3)$ for the high NO_x photochemical experiments (Exp. 3, 4, 4R, and 5). The blue lines show the base model simulation, and the orange lines show simulations where the NO + HO_2→ HNO_3 reaction rate constant was increased by a factor of 10. Shaded regions represent model uncertainty, estimated at ±5.6 % based on the combined uncertainty from chamber wall loss, dilution rates, and $\Delta^{17}O(O_3^{term})$ value. Observations are shown as black markers with error bars. Increasing the NO + HO_2 reaction rate resulted in small changes to the simulated $\Delta^{17}O(HNO_3)$ of -1.6, -0.9, -0.8, and -0.3 ‰ for Exp. 3, 4, 4R, and 5, respectively.

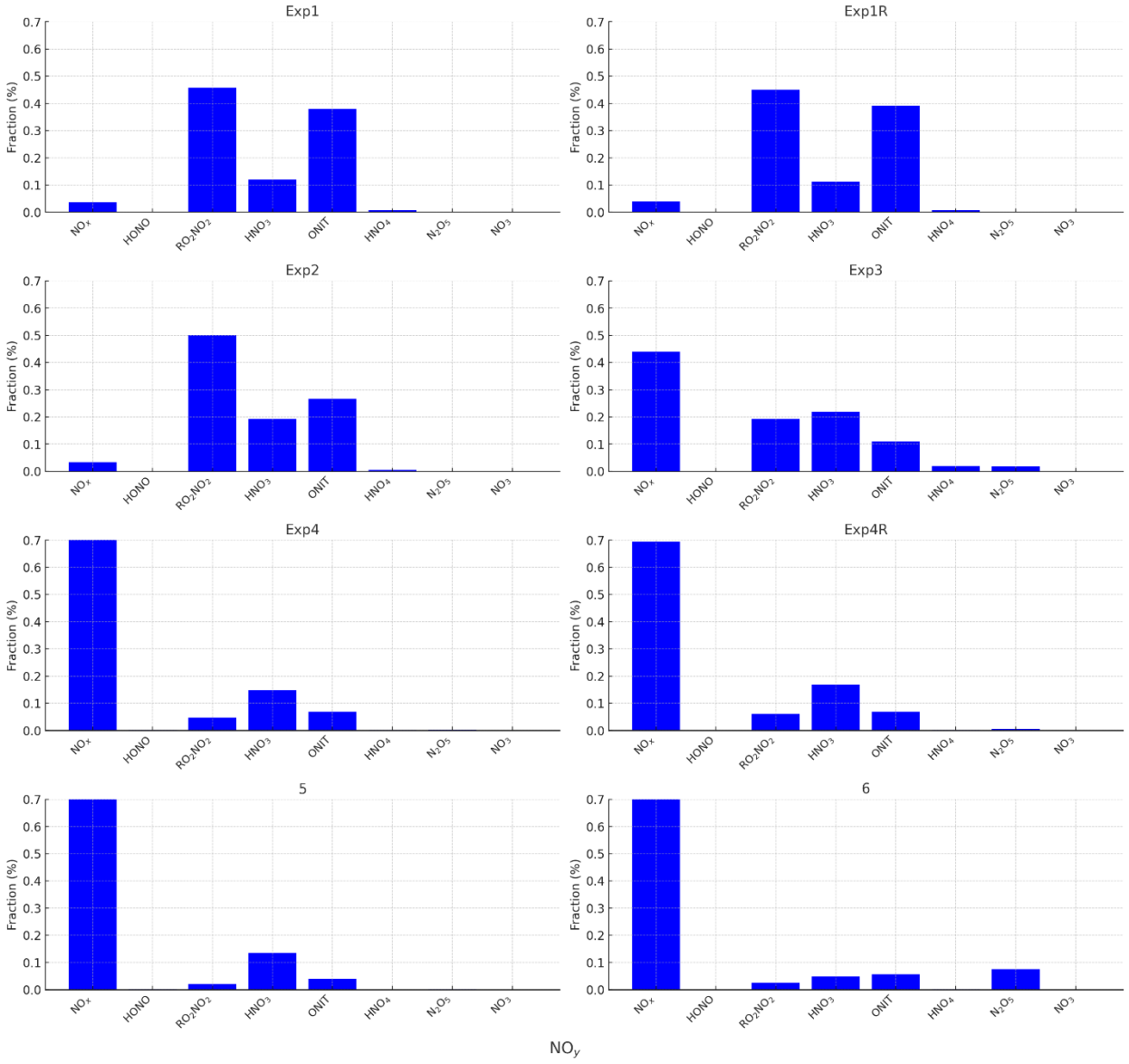

Fig. S10. Breakdown of simulated NO_y components at the time of peak aerosol concentration (corresponding to the start of NO_y collection and chamber dilution) for each experiment (Exp. 1, 1R, 2, 3, 4, 4R, 5, and 6). Fractions are shown for NO_x, HONO, RO_2NO_2, HNO_3, HNO_4, and ONIT. RO_2NO_2 represents the sum of PAN and PINPAN, while ONIT includes ONITa, ONITb, ONITc, ONITOOHa, ONITOOHb, PDN, and DIMER, based on species definitions in the NO_x-API chemical mechanism.

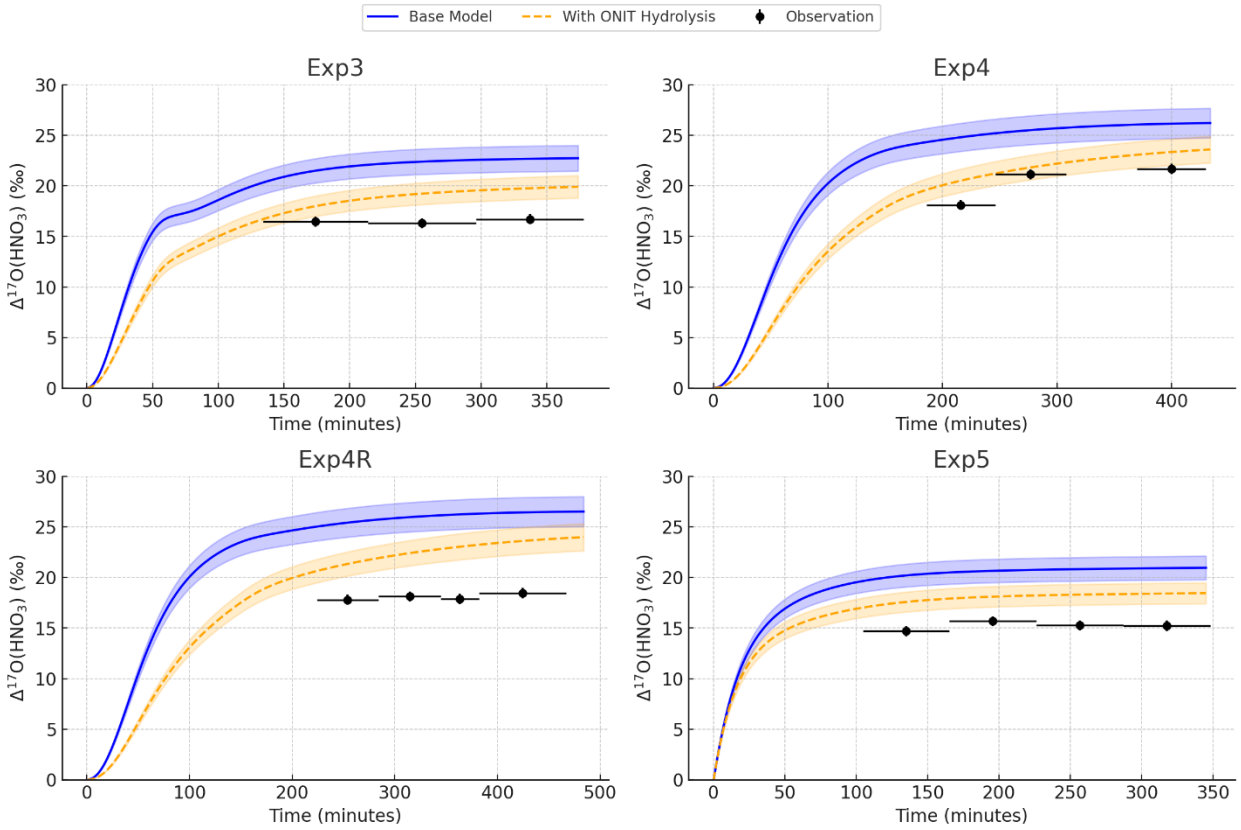

Fig. S11. Modeling and observed $\Delta^{17}O(HNO_3)$ during Experiments 3, 4, 4R, and 5 considering the role of organic nitrate hydrolysis in the model simulations. The blue solid line shows the base model predictions for $\Delta^{17}O(HNO_3)$ with a shaded region representing ±5.6 % model uncertainty. The orange dashed line shows the ONIT Hydrolysis sensitivity simulation, also with ±5.6 % uncertainty. Black points represent observations of $\Delta^{17}O(HNO_3)$.

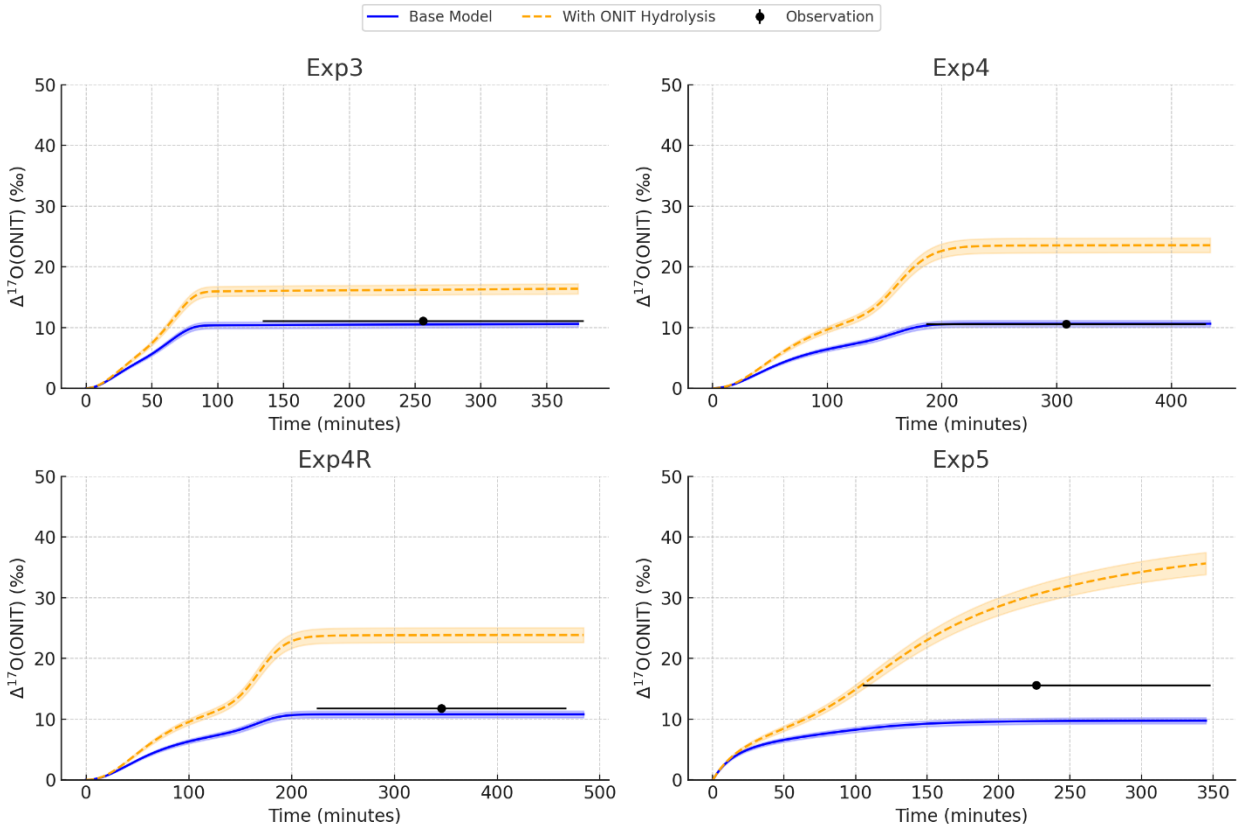

Fig. S12. Modeling and observed $\Delta^{17}O(ONIT)$ during Experiments 3, 4, 4R, and 5 considering the role of organic nitrate hydrolysis in the model simulations. The blue solid line shows the base model predictions for $\Delta^{17}O(ONIT)$ with a shaded region representing ±5.1 % model uncertainty. The orange dashed line shows the ONIT Hydrolysis sensitivity simulation, also with ±5.1 % uncertainty. Black points represent observations of $\Delta^{17}O(pNO_3)$.

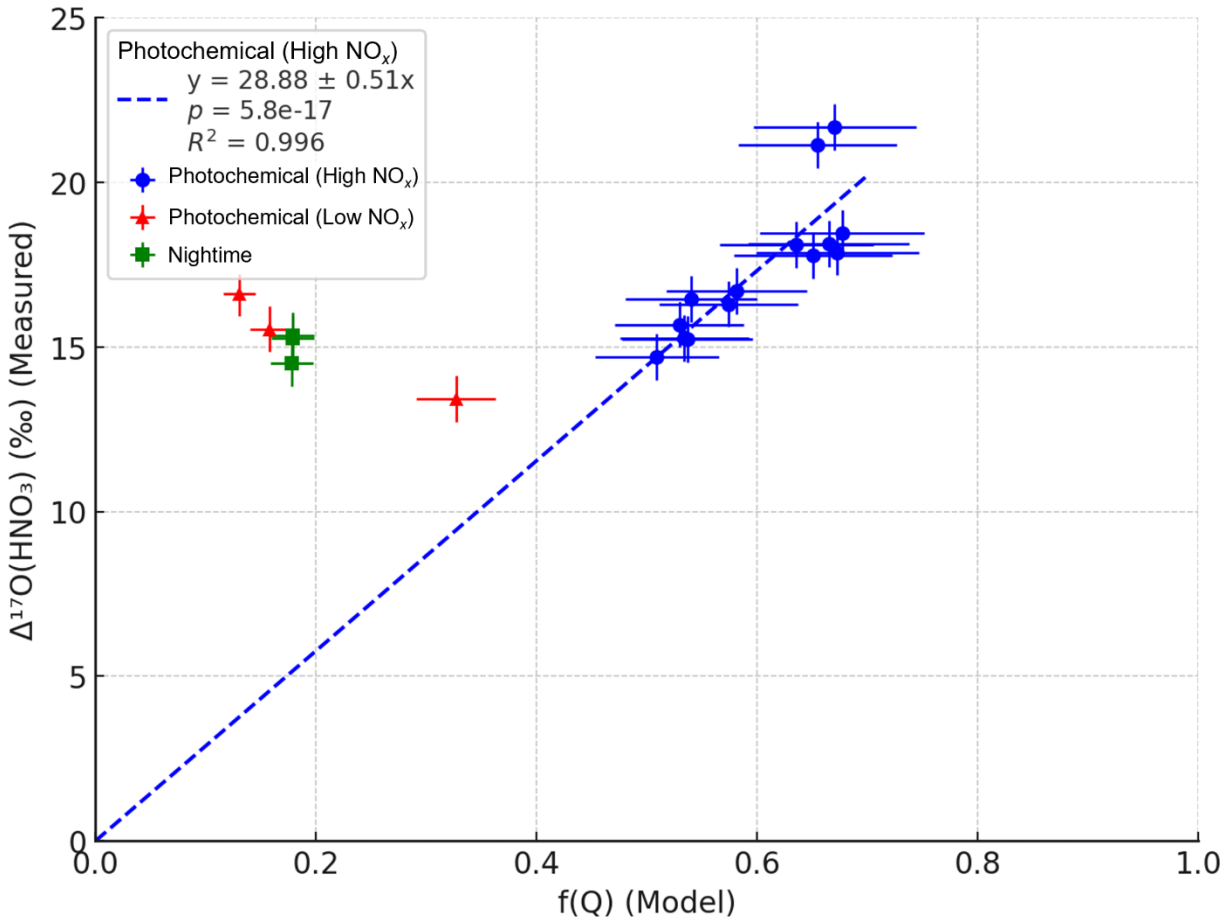

Fig. S13. The measured $\Delta^{17}O(HNO_3)$ as a function of modeled $f(Q)$ in HNO_3 for the high NO_x photochemical, low-NO_x photochemical (Exp 1-2) and nighttime (Exp 6) experiments. A linear regression constrained through the origin was performed on the high NO_x photochemical data only (blue dashed line), yielding a slope of 28.88 ± 0.51. Low-NO_x and nighttime experiments were plotted for reference but were not included in the regression.

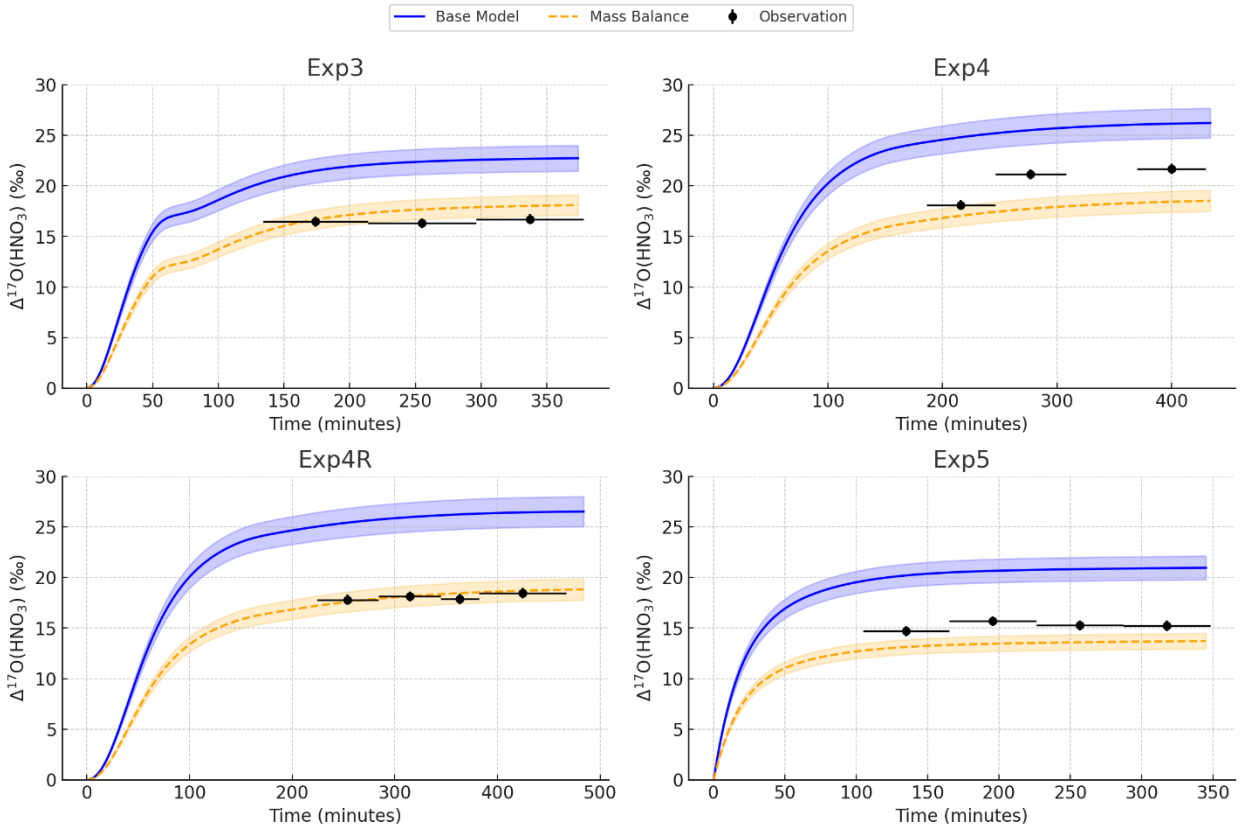

Fig. S14. Time series of $\Delta^{17}O(HNO_3)$ during Experiments 3, 4, 4R, and 5 under the modified NO_2 + OH $\Delta^{17}O$ mass-balance sensitivity simulation of $\Delta^{17}O(HNO_3) = (1/2)\Delta^{17}O(NO_2)$.

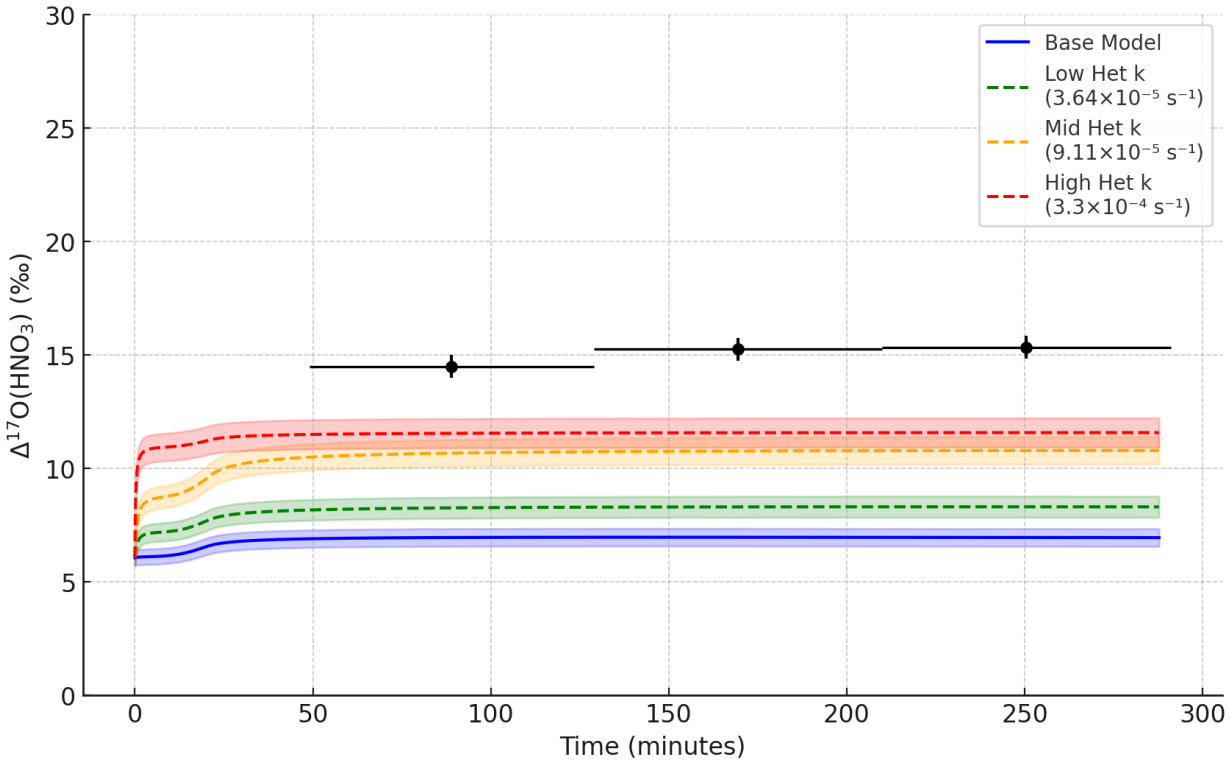

Fig. S15. Modeled $\Delta^{17}O(HNO_3)$ under varying heterogeneous reaction rate constant assumptions compared to observations for the nighttime experiment (Exp 6). Four model scenarios are shown: a base model with no heterogeneous uptake, a low uptake rate constant ($k = 3.64 \times 10^{-5}$ s^{-1}), a moderate uptake rate constant ($k = 9.11 \times 10^{-5}$ s^{-1}), and a high uptake rate constant ($k = 3.3 \times 10^{-4}$ s^{-1}).

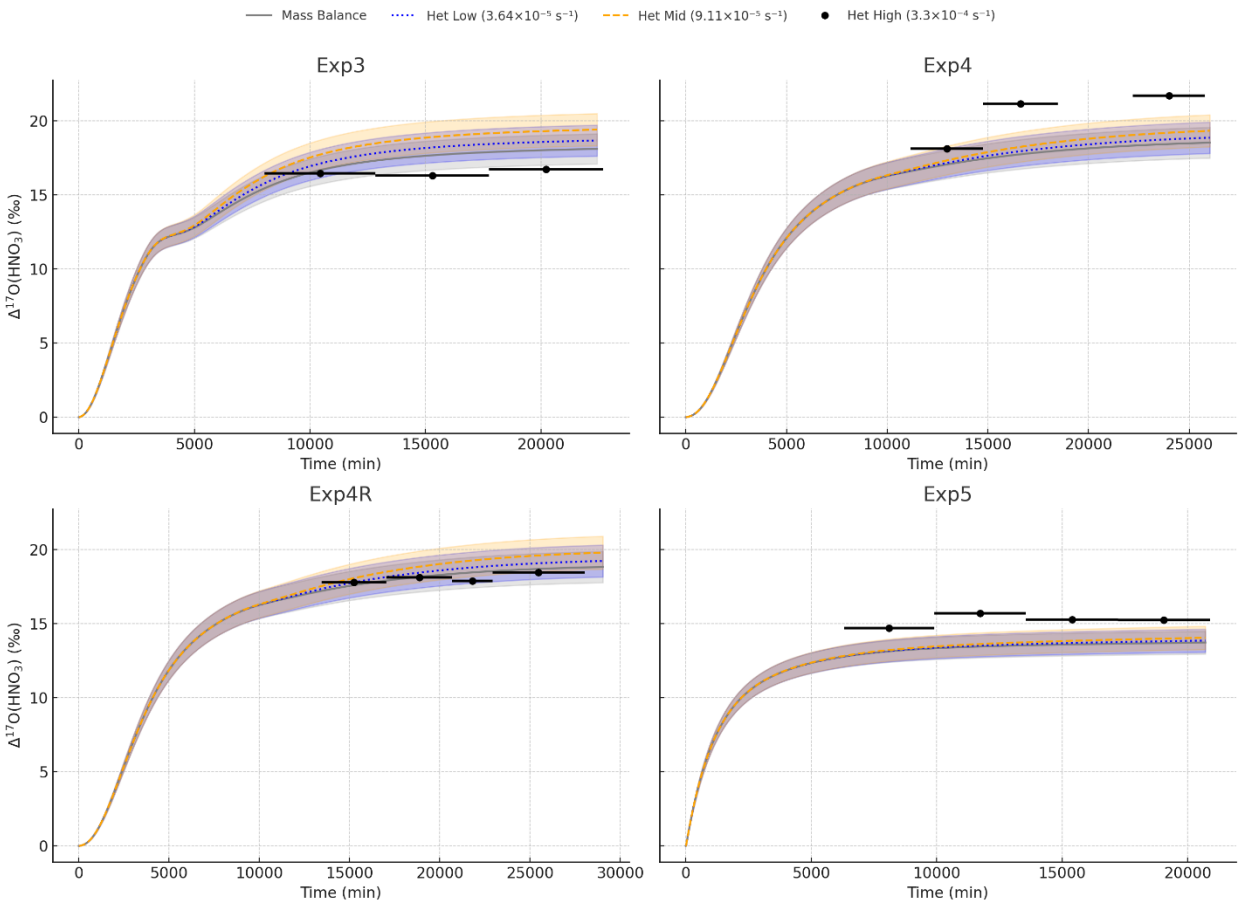

Fig. S16. Modeled $\Delta^{17}O(HNO_3)$ under varying heterogeneous reaction rate constant assumptions compared to observations for the high NO_x photochemical experiments (Exp. 3-5). Four model scenarios are shown: a base model with no heterogeneous uptake, a low uptake rate constant ($k = 3.64 \times 10^{-5}$ s^{-1}), a moderate uptake rate constant ($k = 9.11 \times 10^{-5}$ s^{-1}), and a high uptake rate constant ($k = 3.3 \times 10^{-4}$ s^{-1}). All model simulations inlcuded the updated NO_2 + OH oxygen isotope mass balance of $\Delta^{17}O(HNO_3) = (1/2)\Delta^{17}O(NO_2)$.

Table S1. Summary of the NO_x-API Species List.

Species	Description	SMILES
Inorganic		
CO	Carbon monoxide	C=O
CO_2	Carbon dioxide	O=C=O
H_2	Hydrogen	[H][H]
H_2O	Water Vapor	O
H_2O_2	Hydrogen peroxide	OO
HNO_3	Nitric acid	O=N(=O)O
HO_2	Hydroperoxy radical	[O]O
HO_2NO_2	Pernitric acid	OO[N+](=O)[O-]
HONO	Nitrous acid	O=N[O]
N_2	Molecular nitrogen	N#N
N_2O_5	Dinitrogen pentoxide	O=[N+](=O)O[N+](=O)[O-]
NO	Nitric oxide	[N]=O
NO_2	Nitrogen dioxide	[O-][N+](=O)
NO_3	Nitrate radical	[O-][N+](=O)O
O_2	Molecular oxygen	O=O
$O(^1D)$	Excited state oxygen atom $O(^1D)$	[O]
O_3	Ozone	O=O=O
$O(^3P)$	Ground state oxygen atom $O(^3P)$	[O]
OH	Hydroxl radical	[OH]
Organic		
ACT	Acetone	CC(=O)C
API	A-pinene	C/C1=C/CC2CC1C2(C)C
APINAO	alpha-pinene alkoxy radical	OC1CC2CC(C1(C)[O])C2(C)C
$APINAO_2$	tertiary (major) peroxy radical from APIN + OH + O_2	[O]OC1(C)C(O)CC2CC1C2(C)C
APINAOOH	pinene-derived hydroxy hydroperoxide	OOC1(C)C(O)CC2CC1C2(C)C
APINBO	alpha-pinene alkoxy radical	[O]C1CC2CC(C1(C)O)C2(C)C
$APINBO_2$	secondary (minor) peroxy radical from APIN + OH + O_2	[O]OC1CC2CC(C1(C)O)C2(C)C
APINBOOH	pinene-derived hydroxy hydroperoxide	OOC1CC2CC(C1(C)O)C2(C)C
APINCO	alpha-pinene alkoxy radical	CC1=CCC(CC1O)C(C)(C)[O]
$APINCO_2$	tertiary (minor) peroxy radical from APIN + OH + O_2	[O]OC(C)(C)C1CC=C(C)C(O)C1

APINCOOH	pinene-derived hydroxy hydroperoxide	OOC(C)(C)C1CC=C(C)C(O)C1
DIMER	Dimers from nRO_2 + RO_2 reactions	CC3(C)C4CC(O[N+](=O)O)C(OOC1(C)C(O[N+](=O)O)CC2CC1C2(C)C)C3C4
RO_2	Generic RO_2	N/A
$NAPINAO_2$	tertiary (major) peroxy radical from APIN + NO_3 + O_2;	[O]OC1CC2CC(C1(C)ON(=O)=O)C2(C)C
$NAPINBO_2$	secondary (minor) peroxy radical from APIN + NO_3 + O_2;	[O]OC1(C)C(ON(=O)=O)CC2CC1C2(C)C
ONITa	Tertiary (major) alpha-pinene hydroxynitrate	O=N(=O)OC1(C)C(O)CC2CC1C2(C)C
ONITb	Secondary (minor) alpha-pinene hydroxynitrate	O=N(=O)OC1CC2CC(C1(C)O)C2(C)C
ONITc	Tertiary alpha-pinene carbonyl nitrate	O=N(=O)OC(C)(C)C1CC=C(C)C(O)C1
ONITOOHa	Tertiary alpha-pinene nitrate hydroperoxide	OOC1CC2CC(C1(C)ON(=O)=O)C2(C)C
ONITOOHb	Secondary alpha-pinene nitrate hydroperoxide	OOC1(C)C(ON(=O)=O)CC2CC1C2(C)C
P	Generic Product	N/A
PAN	Peroxyacetyl nitrate	CC(=O)OON(=O)=O
PDN	Pinene dinitrate	CC1(C)C2CC(O[N+](=O)O)C(C)(O[N+](=O)O)C1C2
PINAL	pinonaldehyde	CC(=O)C1CC(CC=O)C1(C)C
$PINO_3$	pinonaldehyde-derived acyl peroxy radical	[O]OC(=O)CC1CC(C(=O)C)C1(C)C
PINPAN	C10 peroxyacyl nitrate	O=N(=O)OOC(=O)CC1CC(C(=O)C)C1(C)C
RO	Generic Aloxy Radical	N/A
RO_3	Generic acyl peroxy radical	N/A

Table S2. Summary of the photolysis reactions* utilized in the NO_x-API Mechanism.

Label	Reaction
R001	$O_3 + h\nu \rightarrow O(^3P) + O_2$
R002	$O_3 + h\nu \rightarrow O(^1D) + O_2$
R003	$H_2O_2 + h\nu \rightarrow OH + OH$
R004	$NO_2 + h\nu \rightarrow O(^3P) + NO$
R005	$NO_3 + h\nu \rightarrow O_2 + NO$
R006	$NO_3 + h\nu \rightarrow O(^3P) + NO_2$
R007	$HONO + h\nu \rightarrow OH + NO$
R008	$HNO_3 + h\nu \rightarrow OH + NO_2$
R009	$HO_2NO_2 + h\nu \rightarrow 0.2\ OH + 0.2\ NO_3 + 0.8\ HO_2 + 0.8\ NO_2$
R058	$PINAL + h\nu \rightarrow RO_2 + CO + HO_2$
R072	$ACT + h\nu \rightarrow RO_3 + RO_2$
R075	$PAN + h\nu \rightarrow RO_3 + NO_2$
R076	$PAN + h\nu \rightarrow RO_2 + NO_3 + CO_2$
R081	$APINAOOH + h\nu \rightarrow P + OH$
R083	$APINBOOH + h\nu \rightarrow P + OH$
R085	$APINCOOH + h\nu \rightarrow P + OH$
R105	$ONITc + h\nu \rightarrow ACT + RO_2 + NO_2$

*The photolysis frequencies (*J*) were calculated inline using the F0AM Box model based on the cross section and quantum yields implemented in MCMv3.2

Table S3. Summary of the thermal reactions utilized in the NO_x-API Mechanism.

Label	Reaction	A $cm^3\ s^{-1}$	E/R K	Reference
Inorganic Reactions				
R010	$O_3 + OH \rightarrow HO_2 + O_2$	1.70×10^{-12}	940	RACM2
R011	$O_3 + HO_2 \rightarrow OH + 2O_2$	1.00×10^{-14}	490	RACM2
R012	$O_3 + NO \rightarrow NO_2 + O_2$	1.40×10^{-12}	1310	RACM2
R013	$NO_2 + O_3 \rightarrow NO_3 + O_2$	1.40×10^{-13}	2470	RACM2
R014	$O^3P + O_2 \rightarrow O_3$	Table S6		
R015	$O^3P + O_3 \rightarrow 2O_2$	8.00×10^{-12}	2060	RACM2
R016	$O^1D + O_2 \rightarrow O^3P + O_2$	3.20×10^{-11}		RACM2
R017	$O^1D + N_2 \rightarrow O^3P + N_2$	1.80×10^{-11}	-107	RACM2
R018	$O^1D + H_2O \rightarrow 2OH$	2.20×10^{-10}		RACM2
R019	$OH + H_2 \rightarrow HO_2 + H_2O$	7.70×10^{-12}	2100	RACM2
R020	$OH + HO_2 \rightarrow H_2O + O_2$	4.80×10^{-11}	-250	RACM2
R021	$HO_2 + HO_2 \rightarrow H_2O_2 + O_2$	Table S6		
R022	$HO_2 + HO_2 + H_2O \rightarrow H_2O_2 + H_2O + O_2$	Table S6		
R023	$H_2O_2 + OH \rightarrow HO_2 + H_2O$	2.90×10^{-12}	160	RACM2
R024	$NO + O^3P \rightarrow NO_2$	Table S4		RACM2
R025	$NO + OH \rightarrow HONO$	Table S4		
R026	$HO_2 + NO \rightarrow OH + NO_2$	3.45×10^{-12}	-270	RACM2
R027	$HO_2 + NO \rightarrow HNO_3$	Table S6		
R028	$NO + NO + O_2 \rightarrow NO_2 + NO_2$	3.30×10^{-39}	-530	RACM2
R029	$HONO + OH \rightarrow NO_2 + H_2O$	2.50×10^{-12}	-260	RACM2
R030	$O^3P + NO_2 \rightarrow NO + O_2$	5.50×10^{-12}	-188	RACM2
R031	$O^3P + NO_2 \rightarrow NO_3$	Table S4		
R032	$OH + NO_2 \rightarrow HNO_3$	Table S4		

R033	$OH + HNO_3 \rightarrow NO_3 + H_2O$	Table S6		
R034	$OH + NO_3 \rightarrow HO_2 + NO_2$	2.00×10^{-11}		RACM2
R035	$HO_2 + NO_3 \rightarrow 0.7\ OH + 0.7\ NO_2 + 0.3\ HNO_3$	4.00×10^{-12}		RACM2
R036	$NO + NO_3 \rightarrow NO_2 + NO_2$	1.80×10^{-11}	-110	RACM2
R037	$NO_2 + NO_3 \rightarrow NO + NO_2 + O_2$	4.50×10^{-14}	1260	RACM2
R038	$NO_3 + NO_3 \rightarrow NO_2 + NO_2 + O_2$	8.50×10^{-13}	2450	RACM2
R039	$NO_2 + NO_3 \rightarrow N_2O_5$	Table S4		
R040	$N_2O_5 \rightarrow NO_2 + NO_3$	Table S5		
R041	$N_2O_5 + H_2O \rightarrow HNO_3 + HNO_3$	2.50×10^{-22}		RACM2
R042	$HO_2 + NO_2 \rightarrow HO_2NO_2$	Table S4		
R043	$HO_2NO_2 \rightarrow HO_2 + NO_2$	Table S5		
R044	$OH + HO_2NO_2 \rightarrow NO_2 + H_2O + O_2$	1.30×10^{-12}	-380	RACM2
R045	$OH + CO \rightarrow HO_2 + CO_2$	Table S6		
API Oxidation				
R046	$API + OH \rightarrow 0.572\ APINAO_2 + 0.353\ APINBO_2 + 0.075\ APINCO_2$	1.2×10^{-11}	-440	MCM
R047	$API + O_3 \rightarrow RO_2 + OH$	8.05×10^{-16}	640	MCM
R048	$API + NO_3 \rightarrow 0.65\ NAPINAO_2 + 0.35\ NAPINBO_2$	1.2×10^{-12}	-490	MCM
$APIO_2$ Rxns				
R049	$APINAO_2 + NO \rightarrow 0.23\ ONITa + 0.77\ PINAL + 0.77\ HO_2 + 0.77\ NO_2$	2.70×10^{-12}	-360	MCM
R050	$APINBO_2 + NO \rightarrow 0.23\ ONITb + 0.77\ PINAL + 0.77\ HO_2 + 0.77\ NO_2$	2.70×10^{-12}	-360	MCM
R051	$APINCO_2 + NO \rightarrow 0.125\ ONITc + 0.875\ ACT + 0.875\ P + 0.875\ NO_2$	2.70×10^{-12}	-360	MCM

R052	$APINAO_2 + HO_2 \rightarrow APINAOOH$	2.66×10^{-13}	-1300	Bates et al.
R053	$APINBO_2 + HO_2 \rightarrow APINBOOH$	2.66×10^{-13}	-1300	Bates et al.
R054	$APINCO_2 + HO_2 \rightarrow APINCOOH$	2.66×10^{-13}	-1300	Bates et al.
R055	$APINAO_2 + NO_3 \rightarrow APINAO + NO_2$	2.3×10^{-12}		MCM
R056	$APINBO_2 + NO_3 \rightarrow APINBO + NO_2$	2.3×10^{-12}		MCM
R057	$APINCO_2 + NO_3 \rightarrow APINCO + NO_2$	2.3×10^{-12}		MCM
PINAL Chemistry				
R059	$PINAL + OH \rightarrow 0.772PINO_3 + 0.228RO_2$	5.2×10^{-12}	-600	MCM
R060	$PINAL + NO_3 \rightarrow PINO_3 + HNO_3$	2.00×10^{-14}		MCM
R061	$PINO_3 + NO \rightarrow RO_2 + NO_2$	7.5×10^{-12}	-290	MCM
R062	$PINO_3 + NO_3 \rightarrow RO_2 + NO_2$	4.00×10^{-12}		MCM
R063	$PINO_3 + NO_2 \rightarrow PINPAN$	Table S4		
R064	$PINO_3 + HO_2 \rightarrow 0.44\ RO_2 + 0.44\ OH + 0.15\ O_3 + 0.55\ P$	2.912×10^{-13}	-980	MCM
R065	$PINPAN \rightarrow PINO_3 + NO_2$	Table S5		
General RO_2 Rxns				
R066	$RO_2 + NO \rightarrow NO_2 + 0.7RO_2 + 0.3P$	2.7×10^{-12}	-360	MCM (from C96O2 + NO)
R067	$RO_2 + HO_2 \rightarrow P$	2.59×10^{-13}	-1300	MCM (from C96O2 + HO_2)
R068	$RO_2 + NO_3 \rightarrow 0.8RO_2 + NO_2 + 0.2P$	2.30×10^{-12}		MCM (from C96O2 + NO_3)
R069	$RO_2 + RO_2 \rightarrow P$	1.30×10^{-12}		MCM (from C96O2 + RO_2)
R070	$RO_2 + PINO_3 \rightarrow P$	1.00×10^{-11}		MCM (from C96CO3 + RO2)
ACT Chemistry				
R071	$ACT + OH \rightarrow RO_2$	Table S6		
PAN Chemistry				
R073	$RO_3 + NO_2 \rightarrow PAN$	Table S4		
R074	$PAN \rightarrow RO_3 + NO_2$	Table S5		

RO_3 Chemistry				
R077	$RO_3 + NO \rightarrow RO_2 + NO_2$	8.10×10^{-12}	-270	RACM2
R078	$RO_3 + HO_2 \rightarrow P$	4.30×10^{-13}	-1040	RACM2
R079	$RO_3 + RO_2 \rightarrow HO_2 + P$	2.00×10^{-11}	-500	RACM2
R080	$RO_3 + RO_3 \rightarrow P$	2.50×10^{-12}	-500	RACM2
APIOOH Chemistry				
R082	APINAOOH + OH $\rightarrow$ P + RO_2	1.83×10^{-11}		MCM
R084	APINBOOH + OH $\rightarrow$ P + OH	3.28×10^{-11}		MCM
R086	APINCOOH + OH $\rightarrow$ P + RO_2	1.03×10^{-10}		MCM
$NAPINO_2$ Chemistry				
R087	$NAPINAO_2 + HO_2 \rightarrow$ 0.37 ONITa + 0.63 PINAL + 0.63 HO_2 + 0.63 OH	2.66×10^{-13}	-1300	MCM
R088	$NAPINAO_2 + NO \rightarrow$ 0.9 PINAL + 1.9 NO_2 + 0.1 ONITa	2.55×10^{-12}	-380	Bates et al.
R089	$NAPINAO_2 + NO_3 \rightarrow$ 0.1 PDN + 0.9 PINAL + 1.8 NO_2	2.30×10^{-12}		MCM
R090	$NAPINAO_2 + NAPINAO_2 \rightarrow$ 0.16 DIMER + 1.68 PINAL + 1.68 NO_2	1.00×10^{-14}		Bates et al.
R091	$NAPINAO_2 + NAPINBO_2 \rightarrow$ 0.34 ONITb + 0.08 DIMER + 1.34 PINAL + 0.08 DIMER + 1.34 NO_2	1.00×10^{-14}		Bates et al.
R092	$NAPINBO_2 + HO_2 \rightarrow$ ONITOOHb	2.66×10^{-13}	-1300	Bates et al.
R093	$NAPINBO_2 + NO \rightarrow$ 0.9 PINAL + 1.9 NO_2 + 0.1 ONITb	2.55×10^{-12}	-380	Bates et al.
R094	$NAPINBO_2 + NO_3 \rightarrow$ 0.1 PDN + 0.9 PINAL + 1.8 NO_2	2.30×10^{-12}		Bates et al.
R095	$NAPINBO_2 + NAPINBO_2 \rightarrow$ 0.68 ONITb + 0.16	1.00×10^{-14}		Bates et al.

	DIMER + PINAL + NO_2			
RO_2 Cross Reactions				
R096	$APINAO_2$ + $APINAO_2$ → 2 PINAL + 2 HO_2	1.00×10^{-14}		Bates et al.
R097	$APINAO_2$ + $APINBO_2$ → 2 PINAL + 2 HO_2	1.00×10^{-14}		Bates et al.
R098	$APINAO_2$ + $APINCO_2$ → 2 PINAL + 2 HO_2	1.00×10^{-14}		Bates et al.
R099	$APINBO_2$ + $APINBO_2$ → 2 PINAL + 2 HO_2	1.00×10^{-14}		Bates et al.
R0100	$APINBO_2$ + $APINCO_2$ → 2 PINAL + 2 HO_2	1.00×10^{-14}		Bates et al.
R101	$APINCO_2$ + $APINCO_2$ → 2 PINAL + 2 HO_2	1.00×10^{-14}		Bates et al.
ONIT Reactions				
R102	ONITa + OH → PINAL + NO_2	5.50×10^{-12}		MCM
R103	ONITb + OH → P + NO_2	3.64×10^{-12}		MCM
R104	ONITc + OH → ACT + P + NO_2	9.87×10^{-11}		MCM

RACM2: (Goliff et al., 2013)
MCM: (Saunders et al., 2003)
Bates et al.: (Bates et al., 2022)

Table S4. The NO_x-API-Mechanism: Troe Reaction Parameters

Label	Reaction	k_0^{300} $cm^6\ s^{-1}$	n	k_∞^{300} $cm^3\ s^{-1}$	m	Reference
R024	$NO + O^3P \rightarrow NO_2$	9.00×10^{-32}	1.5	3.00×10^{-11}	0	RACM2
R025	$NO + OH \rightarrow HONO$	7.00×10^{-31}	2.6	3.60×10^{-11}	0.1	RACM2
R031	$O^3P + NO_2 \rightarrow NO_3$	2.50×10^{-31}	1.8	2.20×10^{-11}	0.7	RACM2
R032	$OH + NO_2 \rightarrow HNO_3$	1.80×10^{-30}	3.0	2.80×10^{-11}	0	RACM2
R039	$NO_2 + NO_3 \rightarrow N_2O_5$	2.00×10^{-30}	4.4	1.40×10^{-12}	0.7	RACM2
R042	$HO_2 + NO_2 \rightarrow HO_2NO_2$	2.0×10^{-31}	3.4	2.90×10^{-12}	1.1	RACM2
R063	$PINO_3 + NO_2 \rightarrow$ PINPAN	9.70×10^{-29}	5.6	9.30×10^{-12}	1.5	RACM2
R073	$RO_3 + NO_2 \rightarrow$ PAN	9.70×10^{-29}	5.6	9.30×10^{-12}	1.5	RACM2

RACM2: (Goliff et al., 2013)

Table S5. The NO_x-API Mechanism: Troe Equilibrium Reactions.

Label	Reaction	A	B	k_0^{300} $cm^6\ s^{-1}$	n	k_∞^{300} $cm^3\ s^{-1}$	m	Reference
R040	$N_2O_5 \rightarrow NO_2 + NO_3$	3.70×10^{26}	11,000	2.20×10^{-30}	3.9	1.50×10^{-12}	0.7	RACM2
R043	$HO_2NO_2 \rightarrow HO_2 + NO_2$	4.76×10^{26}	10,900	2.00×10^{-31}	3.4	2.90×10^{-12}	1.1	RACM2
R065	PINPAN $\rightarrow PINO_3 + NO_2$	1.16×10^{28}	13,954	9.70×10^{-29}	5.6	9.30×10^{-12}	1.5	RACM2
R074	PAN $\rightarrow RO_3 + NO_2$	1.16×10^{28}	13,954	9.70×10^{-29}	5.6	9.30×10^{-12}	1.5	RACM2

RACM2: (Goliff et al., 2013)

Table S6. NO_x-API-Mechanism: Reactions with Special Rate Expressions.

Label	Reaction	Rate Constant Expression $cm^3\ s^{-1}$	Reference
R014	$O^3P + O_2 \rightarrow O_3$	$[M] \times 5.60 \times 10^{-34} \times (T/300)^{-2.6}$	RACM2
R021	$HO_2 + HO_2 \rightarrow H_2O_2 + O_2$	$2.2\times10^{-13} \times\exp(600/T) +1.90 \times10^{-33}\times [M] \times\exp(980/T)$	RACM2
R022	$HO_2 + HO_2 + H_2O \rightarrow H_2O_2 + H_2O + O_2$	$3.08\times10^{-34}\times \exp(2800/T) + 2.59\times 10^{-54} \times [M] \times \exp(3180/T)$	RACM2
R027	$HO_2 + NO \rightarrow HNO_3$	$k_1 = 3.45E\text{-}12*\exp(270/T)$ $k_2 = (530/Y)+(4.8 \times 10^{-6})*pressure - 1.73$ $k = k_1*k_2/100$	RACM2
R033	$OH + HNO_3 \rightarrow NO_3 + H_2O$	$k = k_0 + k_3/(1 + k_3 / k_2)$ $k_0 = 2.4 \times 10^{-14} \times \exp(460/T)$ $k_2 = 2.4 \times 10^{-17} \times \exp(2199/T)$ $k_3 = 6.5 \times 10^{-34} \times \exp(1335/T) \times [M]$	RACM2
R045	$OH + CO \rightarrow HO_2 + CO_2$	$1.44 \times 10^{-13} \times (1 + 0.8 \times [M] / 4 \times10^{19})$	RACM2
R071	$ACT + OH \rightarrow RO_2$	$1.39 \times 10^{-13} + 3.72 \times 10^{-11} \times \exp(-2044/T)$	RACM2

RACM2: (Goliff et al., 2013)

Table S7. The wall-loss reactions and rate coefficients utilized in the wall-loss sensitivity simulations.

Reaction	Rate Constant*	Reference
$O_3 \rightarrow wO_3$	2.19×10^{-6} (s^{-1})	a
$NO \rightarrow wNO$	2.34×10^{-6} (s^{-1})	a
$NO_2 \rightarrow 0.5HONO + 0.5wHNO_3$	2.31×10^{-6} (s^{-1})	a
$HNO_3 \rightarrow wHNO_3$	2.31×10^{-4} (s^{-1})	a
$wHNO_3 \rightarrow OH + NO_2$	$J(HNO_3)$	a
$N_2O_5 + H_2O \rightarrow 2wHNO_3$	1×10^{-20} (cm^3 $molecule^{-1}$ s^{-1})	a
$N_2O_5 \rightarrow 2wHNO_3$	1×10^{-5} (s^{-1})	a
ONITa → *w*ONIT	8.8×10^{-6} (s^{-1})	b
ONITb →*w*ONIT	8.8×10^{-6} (s^{-1})	b
ONITc → *w*ONIT	8.8×10^{-6} (s^{-1})	b
PDN → *w*ONIT	8.8×10^{-6} (s^{-1})	b
DIMER → *w*ONIT	8.8×10^{-6} (s^{-1})	b
ONITOOHa → *w*ONIT	8.8×10^{-6} (s^{-1})	b
ONITOOHb → *w*ONIT	8.8×10^{-6} (s^{-1})	b

[a](Wang et al., 2014)

[b](Morales et al., 2021)

*The wall loss sensitivity simulations were conducted using previously reported rate constants as well as increasing the rate constant by ×10

Table S8. Summary of the organic nitrate hydrolysis reactions incorporated into the NO_x–API mechanism for a sensitivity simulation evaluating the potential contribution of organic nitrate hydrolysis as a source of HNO_3 with a low $\Delta^{17}O$ value. The hydrolysis rate constants were selected to correspond to an organic nitrate lifetime of 30 minutes.

Label	Reaction	Rate constant (k) (s^{-1})
Hydro-01	ONITa → HNO_3+P	5.56×10^{-4}
Hydro-02	ONITb → HNO_3+P	5.56×10^{-4}
Hydro-03	ONITc → HNO_3+P	5.56×10^{-4}
Hydro-04	ONITOOHa → HNO_3+P	5.56×10^{-4}
Hydro-05	ONITOOHb → HNO_3+P	5.56×10^{-4}
Hydro-06	DIMER → $2HNO_3$ + P	5.56×10^{-4}
Hydro-07	PDN → $2HNO_3$ + P	5.56×10^{-4}

Table S9. Summary of the heterogeneous N_2O_5 heterogeneous reaction incorporated into the NO_x-API mechanism for a sensitivity simulation evaluating its contribution to HNO_3 formation. Sensitivity tests were conducted in which the rate constant was varied corresponding to an N_2O_5 lifetime from 0.46 to 4.6 hr.

Label	Reaction	$\Delta^{17}O$ Mass Balance	Rate constant (k) (s^{-1})
Het-01	$N_2O_5 \rightarrow 2HNO_3$	$\Delta^{17}O(HNO_3) = (5/6)\Delta^{17}O(NO_2) + (1/6)\Delta^{17}O(O_3^{term})$	0.6×10^{-4} to 6×10^{-4}

Table 10. Summary of initial chamber HNO_3 concentrations ("blanks") and maximum HNO_3 mixing ratios observed during each experiment. Blank values represent background HNO_3 levels present at the start of each experiment, based on CIMS measurements. These were modeled with a fixed isotopic composition of $\Delta^{17}O = 36.1 \pm 4.0‰$, as constrained by sensitivity tests conducted for Experiments 1, 1R, and 2.

Experiment	HNO_3^{blank} (ppb_v) (±20 %)	Max HNO_3 (ppb) (±20 %)
1	4.3	21.6
1R	3.5	19.7
2	3.2	40.5
3	4.8	67.0
4	5.7	304.1
4R	5.5	67.4
5	9.0	208.5
6	2.3	22.7

Table S11. Reactions included in the sensitivity simulations used to investigate the isotopic influence of background HNO_3 ("HNO_3^{blank}") on $\Delta^{17}O$ values. These reactions represent the reactivity of pre-existing HNO_3 in the chamber.

Label	Reaction
R008	$HNO_3^{blank} \rightarrow OH + NO_2$
R033	$OH + HNO_3^{blank} \rightarrow NO_3 + H_2O$

Table S12. Summary of the measured NO_y isotope data ($\Delta^{17}O$, $\delta^{18}O$, and $\delta^{15}N$) and uncertainties ($\pm\sigma$) for the various conducted experiments.

	NO_2 (‰)			HNO_3 (‰)			pNO_3 (‰)		
Exp	$\delta^{15}N$	$\Delta^{17}O$	$\delta^{18}O$	$\delta^{15}N$	$\Delta^{17}O$	$\delta^{18}O$	$\delta^{15}N$	$\Delta^{17}O$	$\delta^{18}O$
1	-67.8±1.7	13.4±0.7	43.6±1.8	-37.0±1.7	15.6±0.7	49.0±1.8	-79.6±2.4	5.2±0.8	21.7±0.7
1R	-63.3±1.7	10.8±0.7	45.3±1.8	-37.7±1.7	16.6±0.7	49.0±1.8	-76.3±2.6	5.6±0.8	22.3±0.8
2	-68.3±1.7	18.9±0.7	65.8±1.8	-34.3±1.7	13.4±0.7	43.7±1.8	-78.5±1.1	9.2±0.7	29.2±0.6
3	-70.2±1.7	32.4±0.7	92.6±1.8	-32.0±1.7	16.5±0.7	49.5±1.8	-73.1±1.8	11.1±0.8	37.7±0.8
	-71.8±1.7	32.6±0.7	86.6±1.8	-20.1±1.7	16.3±0.7	48.5±1.8			
	-68.7±1.7	31.2±0.7	80.6±1.8	-19.1±1.7	16.7±0.7	49.3±1.8			
4	-67.8±1.7	40.8±0.7	108.7±1.8	-32.8±1.7	18.1±0.7	48.1±1.8	-90.3±1.9	12.0±0.7	42.4±0.8
	-71.0±1.7	39.3±0.7	107.8±1.8	-47.0±1.7	21.1±0.7	60.2±1.8			
	-71.4±1.7	38.6±0.7	112.1±1.8	-49.7±1.7	21.7±0.7	61.3±1.8			
4R	-67.6±1.7	39.6±0.7	107.8±1.8	-29.6±1.7	17.8±0.7	53.9±1.8	-87.5±4.1	11.8±0.9	40.4±1.4
	-62.9±1.7	39.4±0.7	115.3±1.8	-30.6±1.7	18.1±0.7	55.0±1.8			
	-68.2±1.7	40.7±0.7	108.5±1.8	-26.8±1.7	17.9±0.7	52.2±1.8			
	-68.7±1.7	41.2±0.7	108.7±1.8	-26.8±1.7	18.4±0.7	54.7±1.8			
5	-5.5±1.7	39.1±0.7	103.0±1.8	-8.0±1.7	14.7±0.7	48.5±1.8	-22.5±1.0	15.6±0.9	51.0±1.4
	-6.0±1.7	36.9±0.7	100.8±1.8	-6.3±1.7	15.7±0.7	48.3±1.8			
	-6.0±1.7	37.0±0.7	98.0±1.8	-4.0±1.7	15.3±0.7	48.7±1.8			
	-7.1±1.7	38.1±0.7	101.0±1.8	-4.7±1.7	15.2±0.7	46.8±1.8			
6	-46.0±1.7	7.0±0.7	31.2±1.8	-24.8±1.7	14.5±0.7	45.4±1.8	NA	NA	NA
	-45.8±1.7	7.3±0.7	31.7±1.8	-21.6±1.7	15.3±0.7	47.0±1.8			
	-45.5±1.7	7.4±0.7	32.7±1.8	-24.4±1.7	15.3±0.7	45.8±1.8			

References

Bates, K. H., Burke, G. J., Cope, J. D., and Nguyen, T. B.: Secondary organic aerosol and organic nitrogen yields from the nitrate radical (NO3) oxidation of alpha-pinene from various RO_2 fates, Atmospheric Chemistry and Physics, 22, 1467–1482, https://doi.org/10.5194/acp-22-1467-2022, 2022.

Goliff, W. S., Stockwell, W. R., and Lawson, C. V.: The regional atmospheric chemistry mechanism, version 2, Atmospheric Environment, 68, 174–185, https://doi.org/10.1016/j.atmosenv.2012.11.038, 2013.

Morales, A. C., Jayarathne, T., Slade, J. H., Laskin, A., and Shepson, P. B.: The production and hydrolysis of organic nitrates from OH radical oxidation of β-ocimene, Atmospheric Chemistry and Physics, 21, 129–145, https://doi.org/10.5194/acp-21-129-2021, 2021.

Saunders, S. M., Jenkin, M. E., Derwent, R. G., and Pilling, M. J.: Protocol for the development of the Master Chemical Mechanism, MCM v3 (Part A): tropospheric degradation of non-aromatic volatile organic compounds, Atmospheric Chemistry and Physics, 3, 161–180, https://doi.org/10.5194/acp-3-161-2003, 2003.

Wang, X., Liu, T., Bernard, F., Ding, X., Wen, S., Zhang, Y., Zhang, Z., He, Q., Lü, S., and Chen, J.: Design and characterization of a smog chamber for studying gas-phase chemical mechanisms and aerosol formation, Atmospheric Measurement Techniques, 7, 301–313, 2014.